Struct Multidisc Optim (2017) 55:945–957
DOI 10.1007/s00158-016-1547-6

RESEARCH PAPER

An evaluation of simple techniques to model the variation in strain hardening behavior of steel

Sandeep Shetty[1,2] · **Larsgunnar Nilsson**[2]

Received: 14 October 2015 / Revised: 18 July 2016 / Accepted: 20 July 2016 / Published online: 4 August 2016

Abstract It is important to consider variations in material parameters in the design of automotive structures in order to obtain a robust and reliable design. However, expensive tests are required to gain complete knowledge of the material behavior and its associated variation. Consequently, due to time and cost constraints, simplified material scatter modeling techniques based on scatter data of typical material properties provided by the material suppliers are used at early design stages in simulation-based robustness studies. The aim of this paper is to study the accuracy of the simplified scatter modeling methods in representing the real material variation. The simplified scatter modeling methods are evaluated by comparing the material scatter obtained by them to the scatter obtained by complete tensile tests, which are obtained after detailed time-consuming experimental investigations. Furthermore, an accuracy assessment is carried out based on selected responses from an axially-crushed, square tube made from DP600 steel.

Keywords Material scatter · Tensile test · Flow curve · Stochastic simulation

✉ Sandeep Shetty
sandeep.shetty@volvocars.com

Larsgunnar Nilsson
larsgunnar.nilsson@liu.se

[1] Painted Body and Closures, Volvo Car Corporation, 405 31 Gothenburg, Sweden

[2] Division of Solid Mechanics, Linköping University, 581 83 Linköping, Sweden

1 Introduction

Scatter in material properties is one of the main sources of uncertainty, which needs to be accounted for in stochastic design optimization of automotive body structures. During the early design phases of automotive body structures, different materials are considered for the design. Due to time constraints, designers do not have access to detailed material scatter data. The only data available are material specifications which are stated in material standards and basic mechanical properties provided by material suppliers. Consequently, at these stages only approximative scatter modeling techniques are used for robustness studies. However, due to lack of experimental data these approximative modeling methods have also been used in later stages of the design process. For example in (Lönn et al. 2009; Aspenberg et al. 2013; Chen and Koç 2007; Del Prete et al. 2010) variations in material properties are incorporated by simple scaling of the nominal stress–strain curve, where the scaling factor often is based on variation of either the yield stress, $R_{p0.2}$ or the ultimate stress, R_m. Another commonly used simplified approach is to incorporate material scatter by varying the parameters in an analytical material hardening relation (Ledoux et al. 2007; Marretta and Di Lorenzo 2010; Jansson et al. 2008; Müllerschön et al. 2007; Li et al. 2009; Quetting et al. 2012). The above approximations are based on scatter data of a limited number of material properties and may not represent the true characteristics of the material scatter. However, approximation techniques are necessary when there is no access to the actual experimental data, especially at early design phases.

Recently, there have been studies focusing on developing new simple approaches to material scatter representation in FE simulations, Even and Reichert (2010) proposed two approaches to generate stochastic flow curves using scatter data of the material parameters $R_{p0.2}$, R_m and the elongation at

fracture A_{80} provided by the material supplier. In the first approach, new material curves were generated by repositioning the nominal tensile test curve to match $R_{p0.2}$ and R_m of each scatter data set. In the second approach, the authors developed a predictive model having $R_{p0.2}$, R_m and uniform elongation, A_g as inputs to generate stochastic flow curves. A_g is evaluated using A_{80} distribution and the A_g/A_{80} ratio obtained from the tensile test curve.

Although different approximating approaches to incorporating scatter in material properties in FEA have been used in the literature, rather less attention has been paid to benchmarking these approximating methods in representing real material behavior and its associated variation. In Even and Reichert (2010), the authors have benchmarked their method by comparing the stress–strain curves obtained with the curves generated by physical tests. However, none of the above studies have investigated the accuracy of the approximative scatter modeling approaches to response variations as compared to detailed scatter modeling.

The main purpose of this work is to assess the simplified material scatter modeling approaches in representing the physical behavior of a material and its associated variation. The accuracy assessment is carried out by comparing the approximated material scatter data to detailed experimental scatter data. In addition, the accuracy is assessed also on a structural level by predicting the variation of the response of an axially crushed, thin-walled square tube made of dual phase steel DP600. In this study the focus is given to an impact load case, since the impact load case is one of the most critical load cases in vehicle body structure development.

The article is organized as follows: First, a detailed analysis of the experimental data is performed. Then the material scatter modeling methods are briefly explained. The application example and the results obtained are presented in Section 4 and Section 5 respectively. Finally, a discussion part is presented before conclusions are drawn.

2 Statistical analysis of experimental data

In this study, tensile test results from 102 samples of virgin DP600 material have been used in order to generate representative material scatter data, which will be used in this study as a reference data set. All test specimens are from different coils from the same material supplier and test data concerning the material rolling direction is considered for this study. The nominal thickness of the sheets studied is 1.45 mm and the sample thicknesses are in the range of 1.36-1.55 mm. Dual phase (DP) steels are high strength steels, which consists of two phases namely ferrite and martensite. They are produced by controlled cooling from the austenite phase. Their high strength combined with excellent drawability make them suitable for many automotive structural applications.

2.1 Mechanical properties

Variations of important mechanical properties of DP600 obtained from the tensile tests are listed in Table 1 together with the material specifications according to the VDA 239–100 standard (VDA 2011). For the current sample size 95 % confidence interval of the mean and standard deviation estimates have also been evaluated. See e.g. (Haldar and Mahadevan 2000) for more details. Five mechanical properties, namely proof stress at 0.2 % plastic strain, $R_{p0.2}$, ultimate stress, R_m, strain at rupture with 80 mm gauge length, A_{80}, uniform elongation, A_g, and strain hardening exponent , n, are presented in Table 1. As can be seen, experimentally-observed variations in material properties are within the specified tolerances of the standard. The mean $R_{p0.2}$ nearly matches the median of the specified tolerance for $R_{p0.2}$ by the standard, whereas the mean of R_m differs slightly from the median of the specified tolerance for R_m. The mean and standard deviation of the material parameters are evaluated, assuming a normal distribution.

Table 1 Stochastic mechanical properties of DP600 obtained from tensile tests

	$R_{p0.2}$ [MPa]	R_m [MPa]	A_{80} [%]	A_g [%]	n_{10-15} [−]
Standard specifications	330 - 430	590 - 700	≥20		>0.14
Mean value	377.41	631.80	26.02	17.27	0.1894
95 % Confidence interval	[374.70-380.11]	[628.98-634.63]	[25.78-26.27]	[17.15-17.40]	[0.1879-0.1909]
Standard deviation	13.77	14.38	1.23	0.63	0.008
95 % Confidence interval	[12.11-15.97]	[12.64-16.68]	[1.09-1.43]	[0.55-0.73]	[0.007-0.009]
Minimum value	340.39	596.61	22.77	15.42	0.17
Maximum value	421.28	671.76	28.48	18.74	0.202

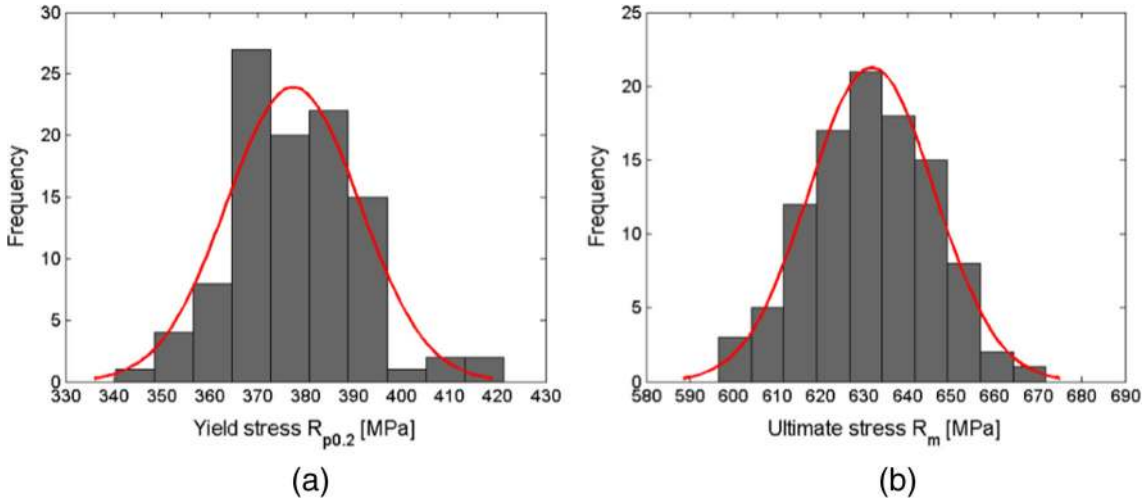

Fig. 1 $R_{p0.2}$, R_m distribution and fitted Gaussian curves for **a** $R_{p0.2}$ and **b** R_m

2.2 Normality test

Normality of the $R_{p0.2}$ and R_m data distributions has been evaluated by the Anderson-Darling test (Anderson and Darling 1952). The test accepts normality for both properties. Furthermore, a check of the data distribution of $R_{p0.2}$ and R_m has been performed by comparing the empirical distribution of the samples with the fitted theoretical normal distribution, see Figs. 1 and 2. As can be seen in Fig. 1, there is a good agreement between the data distribution and the fitted normal density function. The cumulative plots also confirm this, see Fig. 2.

2.3 Correlation matrix

Correlation between material properties has previously been used in some studies to model material scatter efficiently (Even 2010; Wiebenga et al. 2014). Consequently, the correlation between important material parameters has been studied in this section. The correlation coefficients between the material parameters $R_{p0.2}$, R_m, A_{80}, n and the thickness of the sheet are presented in Fig. 3. The Pearson's correlation coefficient is utilized in order to represent the interdependency of the material parameters. The Pearson's correlation coefficient indicates the degree of linear relationship between two variables and it is defined as

$$\rho_{xy} = \frac{Cov(X,Y)}{\sigma_x \sigma_y} \tag{1}$$

where $Cov(X, Y)$ is the covariance between X and Y, σ_x, and σ_y are the standard deviations of X and Y, respectively. Cohen's standard (Cohen 1988) is used in order to determine the strength of the relationship based on the correlation coefficient. As can be seen $R_{p0.2}$ has a medium positive correlation with R_m and a medium negative correlation with A_{80}. A strong negative correlation is found between $R_{p0.2}$ and n. The thickness is weakly correlated to all other parameters. A_{80} has a medium negative correlation with R_m and a strong positive correlation with n.

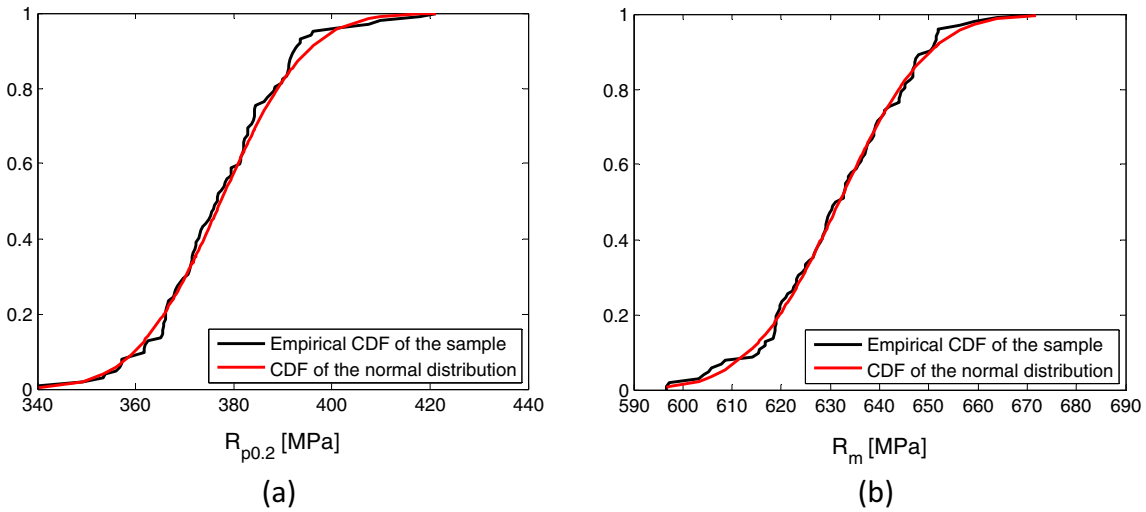

Fig. 2 Cumulative plot of sample distribution and theoretical normal distribution for **a** $R_{p0.2}$ and **b** R_m

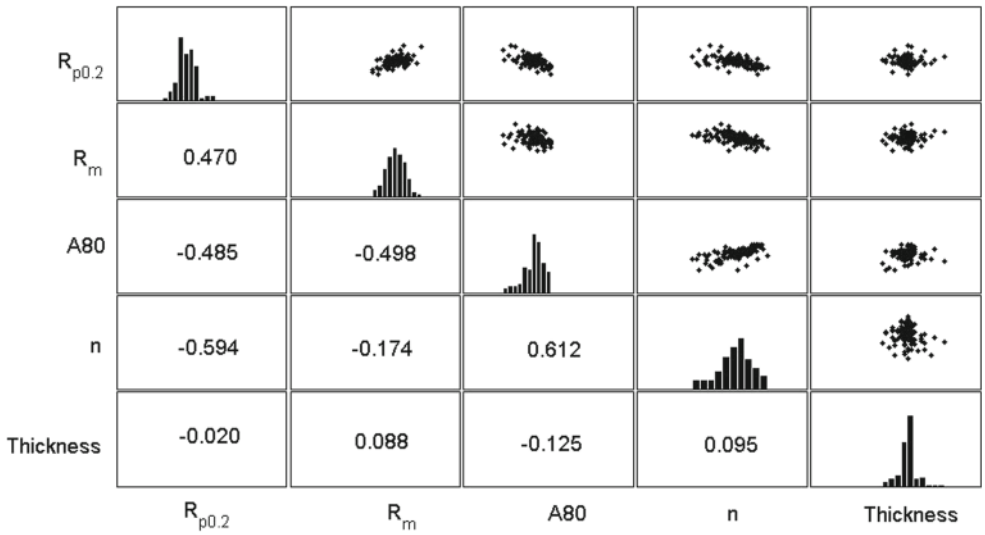

Fig. 3 Correlation matrix

3 Material scatter modeling methods

In this study, seven simple material scatter modeling approaches have been evaluated. The performance of these methods is compared with that of the Direct method, which is based on the actual stress–strain curves obtained by the tensile tests and which here is assumed to represent the true scatter. A set of stochastic flow curves is generated using the methods presented in order to represent the material scatter.

3.1 Direct method

In this method stochastic strain hardening curves are generated using the actual stress–strain curves from uniaxial tensile tests. The engineering stress–strain curves from the tensile tests are presented in Fig. 4.

Standard tensile tests can only capture stress–strain relations accurately during uniform elongation and the stress–strain relation beyond necking can be obtained either by performing additional tests, e.g. shear tests, or by inverse analysis of the tensile tests. Numerous analytical material hardening relations have been published which can be used to extrapolate the data. Apart from extrapolation, analytical approximation also reduce the noise found in experimental data. Two analytical functions, the extended Voce and the Hollomon relations, are here combined in order to describe the plastic strain hardening, as in Larsson et al. (2011). The reason for using the Hollomon hardening function beyond the necking point is that the Voce hardening function yields a good fit up to necking but for higher plastic strains the function saturates and experimental data shows that DP steels exhibit sustained hardening behavior beyond necking (Lee et al. 2005). The combined analytical function is given as

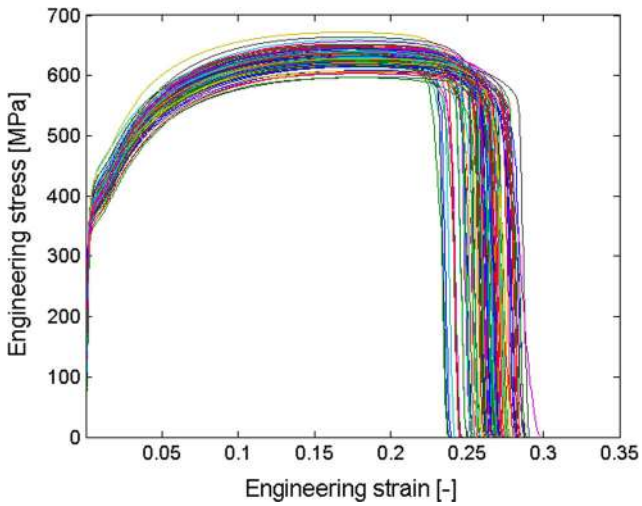

Fig. 4 Engineering stress–strain curves from experiments

$$\sigma_y(\varepsilon_p) = \begin{cases} \sigma_0 + Q_1\left(1-e^{-C_1\varepsilon_p}\right) & \varepsilon_p \le \varepsilon_p^t \\ A + B\left(\varepsilon_p\right)^n & \varepsilon_p^t \le \varepsilon_p \end{cases} \tag{2}$$

where σ_0, Q_1, C_1, A, B and n are material parameters and ε_p^t is the plastic strain at the transition between Voce and Hollomon hardening. A plastic strain close to the diffuse necking point is selected as the transition strain, cf. (Larsson et al. 2011).The parameters of the Voce function for each test curve are fitted using optimization, where the parameters are found by minimizing the error between the Voce fitted curve and the test curve. In order to maintain the smooth transition between the Voce and Hollomon hardening, A, B and n need to satisfy C^1 continuity. Thus,

$$\begin{aligned} A + B\left(\varepsilon_p^t\right)^n &= \sigma_0 + Q_1\left(1-e^{-C_1\varepsilon_p^t}\right) \\ n\ B\ \left(\varepsilon_p^t\right)^{n-1} &= C_1 Q_1 e^{-C_1\varepsilon_p^t} \end{aligned} \tag{3}$$

Furthermore, the flow stress σ_{100} at 100 % plastic strain is introduced in order to evaluate the hardening parameters A, B

and n in Eq. (3), which yields that the condition $A+B=\sigma_{100}$ must be fulfilled. For additional details, see Larsson et al. (2011). Inverse analysis based optimization is carried out in order to determine the optimum value of σ_{100}. The parameters Q_1, C_1, σ_0 and the initial value of σ_{100} is passed to a Matlab routine within the optimization loop. For each plastic hardening curve, the parameters A, B and n are determined by minimizing the mean square error between the experimental force-displacement curve and the force-displacement curve obtained by an FE simulation of the tensile test in LS-DYNA code (Hallquist 2006). A flow chart of the optimization process is presented in Fig. 5. The optimization formulation is given by

$$\begin{aligned} &Find\ \sigma_{100} \\ &Minimize\ e = \sum_{i}^{nd} \left(F^{sim} - F^{exp}\right) \\ &Subject\ to\ \sigma_{100} \geq \sigma_0 + Q_1\left(1-e^{-C_1}\right) \\ &C_1 \leq 1 \end{aligned} \tag{4}$$

where F^{sim} and F^{exp} are the forces obtained from the FE simulation and experiments, respectively. The forces are evaluated at a finite number of displacements nd. The stress–strain curve which approximately represents the average of the fitted set of curves is considered as the nominal stress–strain curve.

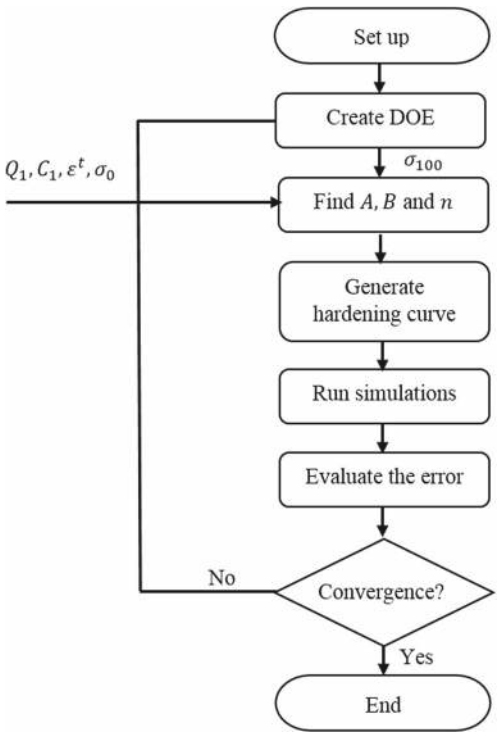

Fig. 5 Flow chart of the optimization process to find σ_{100}

3.2 Approximate methods

In this section, five commonly used simple approximate scatter modeling methods are described. These methods are based on scatter data of a limited number of standard material properties and can thus be used even with basic data from any supplier. Furthermore, two additional approximate methods are introduced in this section. These two methods are proposed for modeling the material scatter data, when the nominal tensile test curve is unavailable. In the first four methods, i.e. Method 1a, Method 1b, Method 2a and Method 2b, scatter data is generated by simple scaling of the nominal stress–strain curve. In the first two methods the nominal stress–strain curve is generated using material standard data, whereas the latter two methods utilize the nominal stress–strain curve from the tensile-test. In Method 3, scatter data is generated by altering the paramters of the analytical material hardening relation. In Method 4 scatter data is generated by interpolation between min and max hardening curves. The correlation between materials parameters has been considered in Method 5 while modeling the material scatter.

3.2.1 Method 1a

The idea behind this approach is to generate stochastic flow curves using the material specifications found in material standards, see Table 1. Thus no additional experimental data is required. In this method stochastic flow curves are generated by scaling the nominal stress–strain curve, c.f. (Lönn et al. 2009; Aspenberg et al. 2013; Chen and Koç 2007; Del Prete et al. 2010). The nominal stress–strain curve is generated using the power law hardening relation

$$\sigma = K\varepsilon^n \tag{5}$$

In the above equation, the value of the strength coefficient K is found from the average value of R_m, for cold rolled DP600 in the VDA 239–100 standard (VDA 2011), while ε and n are kept constant during this evaluation. The true strain at the onset of necking is considered to be equal to the strain hardening exponent. The values of ε and n are set to 0.14, i.e. the lowest n value from the standard specification (VDA 2011). This will yield a conservative estimate of the strain hardening. The mean true R_m is evaluated using the mean engineering R_m from the standard specifications and it is found to be 735 MPa. The nominal plastic hardening curve is then generated by removing the elastic part of the above nominal curve.

The stochastic curves are generated by scaling the nominal stress–strain curves, based on the $R_{p0.2}$ scatter as used in many previous studies. In this work, the $R_{p0.2}$ values are assumed to be normally distributed between the specified tolerance 330–430 MPa, see Table 1. Based on

this data, the mean and standard deviation of the scaling factors are computed. Figure 6 shows the fitted nominal curve in this method along with the nominal stress–strain curve from the Direct method. The nominal curve is fitted using Eq. (5). Figure 7 shows the scaled curves with maximum and minimum scaling factors together with the stochastic flow curves from the Direct method. These scaled curves are generated by scaling the nominal curve using the minimum and maximum scaling factor.

3.2.2 Method 1b

This method uses the same approach as Method 1a except that the scaling factors are based on the scatter in R_m. The mean and the standard deviation of the scaling factor are found using the standard data, see Table 1. The scaled curves with maximum and minimum scaling factor obtained using Method 1b are shown in Fig. 8.

3.2.3 Method 2a

In this method stochastic flow curves are generated by scaling the nominal stress–strain curve as in Method 1a. The only difference is that the nominal stress–strain curve is based on the complete hardening curve from a tensile test. The average stress–strain curve which approximately represents the average of the fitted set of curves in the Direct method is considered as the nominal stress–strain curve. Thus, this method requires the nominal stress–strain curve based on a tensile test apart from standard material data. Here, the scaling factors are based on the scatter in $R_{p0.2}$. The scaled curves with maximum and minimum scaling factors evaluated using Method 2a are presented in Fig. 9. These scaled curves are generated by scaling the nominal curve from the Direct method using the minimum and maximum scaling factor.

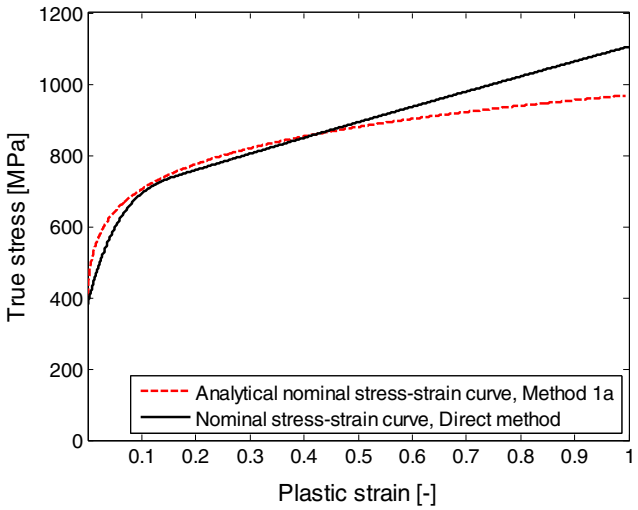

Fig. 6 Nominal stress-train curve using the Direct method and Method 1a

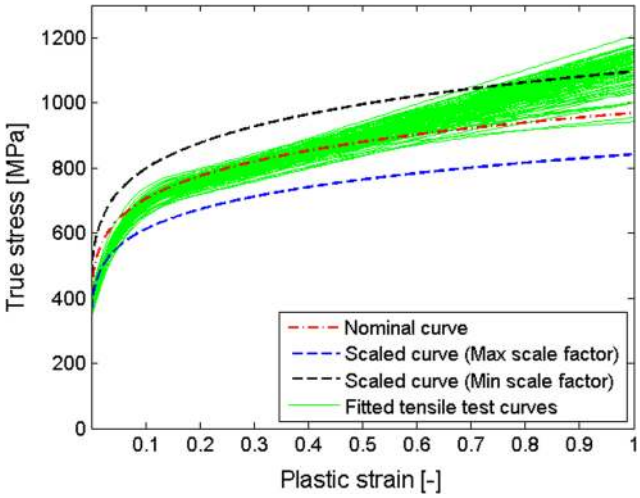

Fig. 7 Scaled curves based on the $R_{p0.2}$ scatter using Method 1a

3.2.4 Method 2b

Method 2b is similar to Method 2a, however the scaling factors are based on the R_m scatter. The scaled curves with maximum and minimum scaling factors evaluated using Method 2b are presented in Fig. 10.

3.2.5 Method 3

In several previously-published studies, material scatter is incorporated by independently varying the parameters in a material hardening description. In (Marretta and Di Lorenzo 2010) the authors have varied the parameters of the power law hardening relation independently to generate stochastic flow curves. These authors have also considered the variations in the anisotropy coefficients and Young's modulus. Whereas, in (Müllerschön et al. 2007) stochastic flow curves are generated by varying the hardening exponent,n, and strength coefficient, K, in the Swift hardening relation. Voce equation is used in (Li

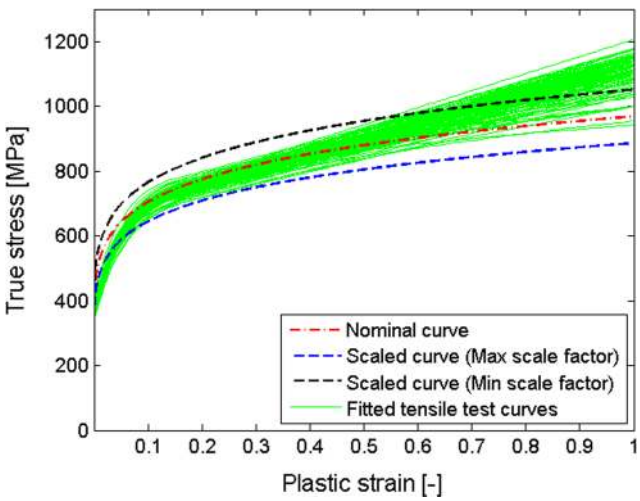

Fig. 8 Scaled curves based on the R_m scatter using Method 1b

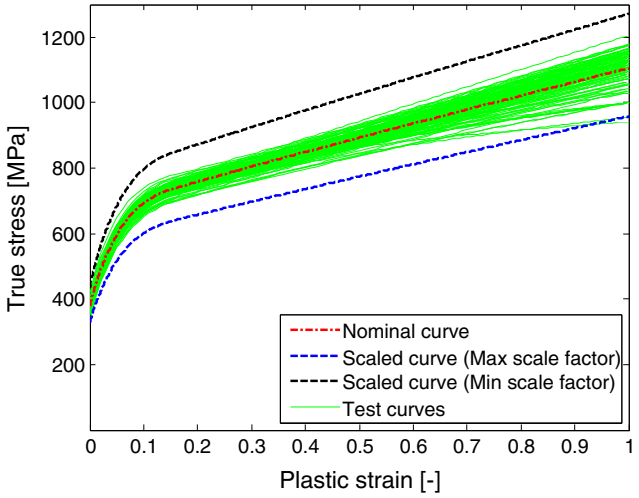

Fig. 9 Scaled curves based on the $R_{p0.2}$ scatter using Method 2a

et al. 2009) to fit a nominal tensile test curve, and stochastic curves are created by varying one parameter and keeping the other parameters constant. Quetting et al. (2012) proposed two approaches to incorporate material scatter in which stochastic flow curves are generated by varying four material parameters $R_{p0.2}$, R_m, n and A_g in the hardening relations. The authors' of (Quetting et al. 2012) have used two hardening relations, which are based on the Ghosh and Hocket-Sherby formulations, respectively. In Sigvant and Carleer (2006), the nominal stress–strain curve is approximated with an equation and stochastic flow curves are generated by independently varying the values of R_m and $R_{p0.2}$ in the fitted equation.

The presented method in this section is similar to those used in the above studies. In this method stochastic hardening curves are generated by independently varying the hardening exponent, n, and the strength coefficient, K, of the power law hardening function, cf. Eq. (5). Since the scatter in the hardening exponent, n, is not listed in the standard material specifications, this data is obtained from the material supplier. The mean and standard deviation of the hardening exponent, n, is computed based on the n scatter data obtained and it is assumed that the variation of n is normally distributed. The mean value of n for the present material is found to be 0.20 and the standard deviation is 0.008. The mean and standard deviation of K are evaluated from Eq. (5) using the mean and standard deviation of R_m, while ε and n both are kept constant at 0.20 during this evaluation. The mean true R_m is evaluated using the strain at ultimate strength and the mean engineering R_m from standard data. The mean true R_m is found to be 774 MPa and this leads to $K = 1067$ MPa for $n = 0.20$. The standard deviation of $R_m = 18.33$ MPa leads to the standard deviation of $K = 25.29$ MPa. The plastic hardening curves are generated by removing the elastic part of the stochastic stress–strain curves generated. The nominal stress–strain curve is generated using Eq. (5) and it is shown in Fig. 11.

3.2.6 Method 4

In this method stochastic hardening curves are generated by interpolation between two curves which represent the upper and lower bounds of the hardening curve spectrum from the experiments, see Fig. 12. The representative curves are created using the Swift hardening relation.

$$\sigma = K\left(\varepsilon_0 + \varepsilon_p\right)^n \tag{6}$$

where K, ε_0, n are material parameters and ε_p is the effective plastic strain. The material parameters of the Swift curve are evaluated using the actual stress–strain curves, which represent the upper and lower bounds of the test curve spectrum. These parameters are found by minimizing the error between the fitted Swift curve and the actual test curve. The nominal stress–strain curve

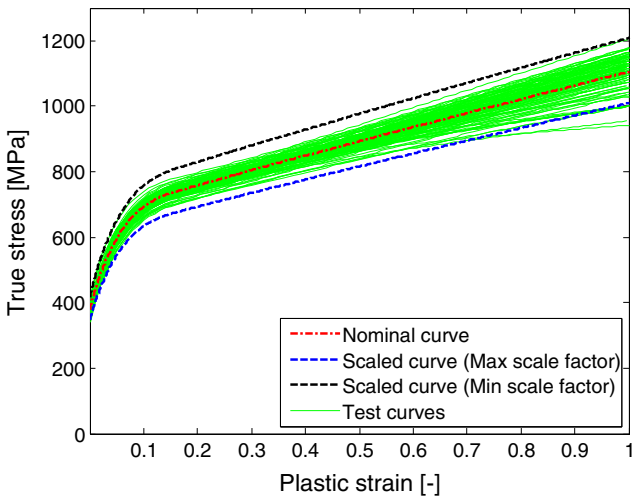

Fig. 10 Scaled curves based on the R_m scatter using Method 2b

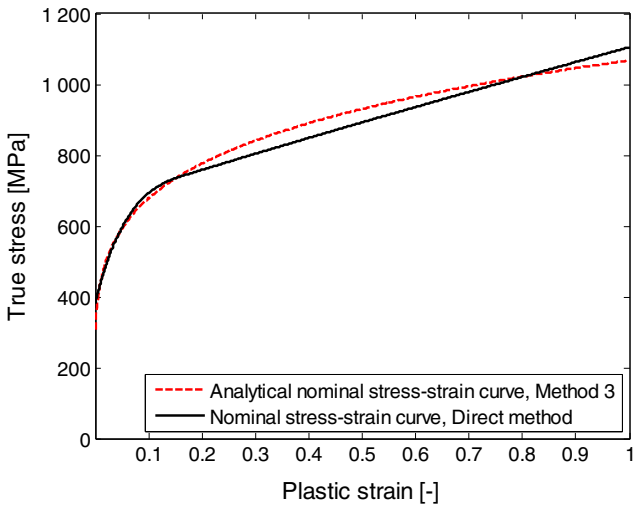

Fig. 11 Nominal stress-train curve using the Direct method and Method 3

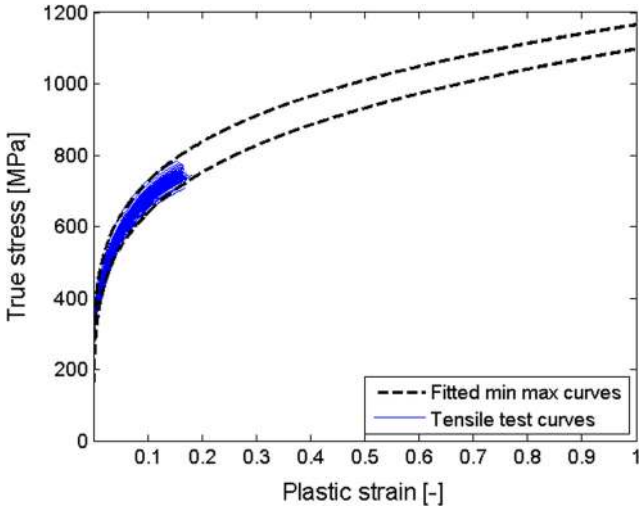

Fig. 12 Experimental stress–strain curves and binding analytical curves using Method 4

from the Direct method and the average curve generated using Method 4 are presented in Fig. 13.

3.2.7 Method 5

The correlation observed between the material parameters has been used in some of the previously-published studies in order to improve the efficiency of material scatter modeling, e.g. (Even 2010; Wiebenga et al. 2014). In the method presented by Even and Reichert (2010), they utilized the correlation between $R_{p0.2}$ and R_m to model R_m as a linear function of $R_{p0.2}$. Since only a moderate correlation between $R_{p0.2}$ and R_m is observed, in this study a Gaussian Copula-based (Embrechts et al. 2001) approach is used in order to model the dependencies between these two parameters. A Copula is a function that connects a multivariate distribution to its univariate marginals.

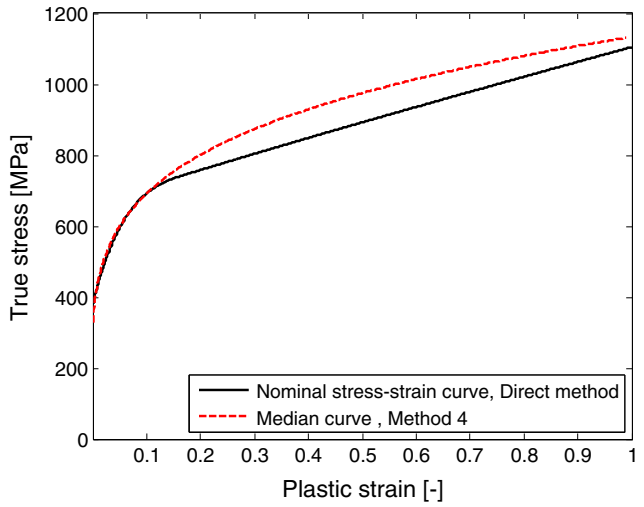

Fig. 13 Nominal stress-train curve using the Direct method and the average stress–strain curve using Method 4

The Gaussian copula for a bivariate case is given by

$$C_N(u.v) = \int_{-\infty}^{\Phi^{-1}(u)} \int_{-\infty}^{\Phi^{-1}(v)} \frac{1}{2\pi\left(1-R_{12}^2\right)^{1/2}} exp\left\{-\frac{s^2-2R_{12}st+t^2}{2\left(1-R_{12}^2\right)}\right\} dsdt \tag{7}$$

where Φ^{-1} denotes the inverse of the standard univariate normal distribution, u (0, 1) is the uniformly distributed marginal and R_{12} is the linear correlation coefficient between the two random variables. In this study, the distribution of R_m given $R_{p0.2}$ is generated by a conditional distribution of the bivariate Gaussian copula using Cholesky decomposition, see (Embrechts et al. 2001) for more details. The R_m distribution is converted to original scale using

$$R_m = u_2 * std\left(R_{p0.2}\right) + mean(R_m) \tag{8}$$

Once the R_m distribution is known, the stochastic hardening curves are generated using the power law hardening relation as in Method 3. The only difference is that only the value of the strength coefficient, K, is varied and the hardening exponent n is kept constant in Eq. (5). The mean and standard deviation of K are evaluated from Eq. (5) using the mean and standard deviation of R_m. The value of n is set to 0.20 as in Method 3. The mean and standard deviation of the engineering R_m is determined using the R_m distribution obtained by Eq. (8). The mean engineering R_m was found to be 633.3 MPa and the standard deviation 15.06 MPa. The true mean R_m was found to be 759.91 MPa and this leads to K = 1048.5 MPa and the standard deviation of K = 15.06. The nominal curve generated by Method 5 is shown in Fig. 14.

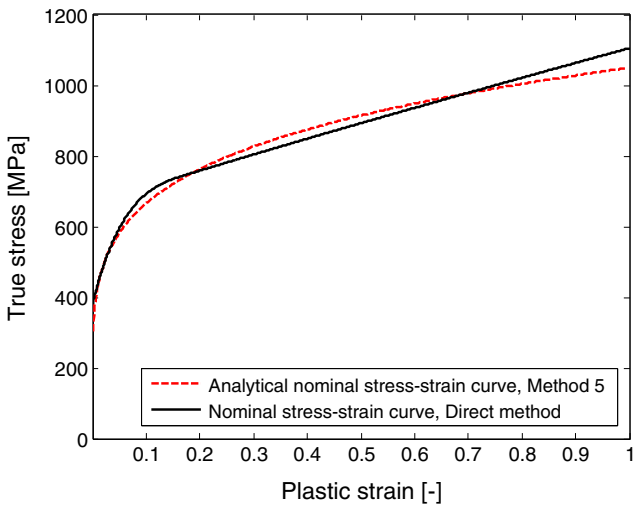

Fig. 14 Nominal stress-train curve using the Direct method and Method 5

4 Application example

Thin-walled tube structures subjected to axial buckling have been widely used as energy absorbers in automotive structures and represent an important type of structural members. In this work, scatter modeling approaches are compared based on the selected responses of an axially-crushed, thin-walled square tube made from DP600 steel. The structural responses considered in this work are the absorbed energy, *AE*, the peak force, F_{peak}, the maximum displacement of the impactor, D_{max}, and the average force, F_{avg}, between 0 and 10 ms. The length of the square tube is 250 mm, the width is 50 mm and the nominal thickness is 1.45 mm, see Fig. 15. The impactor mass is 100 kg and the impact velocity is 8 m/s.

Two triggers are created near the impact end of the tube in order to control the initial bucking deformation. Similar triggers are used in Abedrabbo et al. (2009). The other end of the tube is fixed. The tube is modeled using quadratic Belytschko-Tsay shell elements with 1.5 mm side length. The interface between the impactor and the tube is modeled with the nodes-to-surface contact type and the Coulomb friction coefficient is set to 0.25 to prevent sliding. Self-contact of the tube is considered with the Coulomb friction coefficient set to 0.1 to prevent penetration but allow sliding between the folds. The material is modeled using the piece-wise linear hardening J2 plasticity material model in LS-DYNA (Hallquist 2006). In this study, the effect of strain rate of the material is not considered.

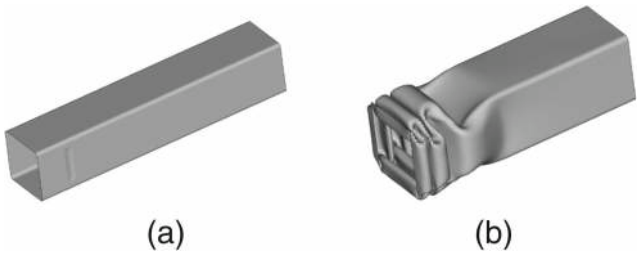

Fig. 16 **a** Undeformed **b** Deformed shape of the tube

The nominal crush behavior of the axially-loaded square tube is presented in Figs. 16 and 17. The undeformed and deformed shapes of the tube specimen are shown in Fig. 16, whereas Fig. 17 shows the crushing force-displacement curve. The nominal response values are presented in Table 4.

Stochastic analysis of the tube is performed using complete set of fitted hardening curves from the tensile tests. Since this analysis is based on the stress–strain curves from the physical tensile tests, the results obtained by this method are considered as the basis for the comparison of the subsequent approximation techniques described.

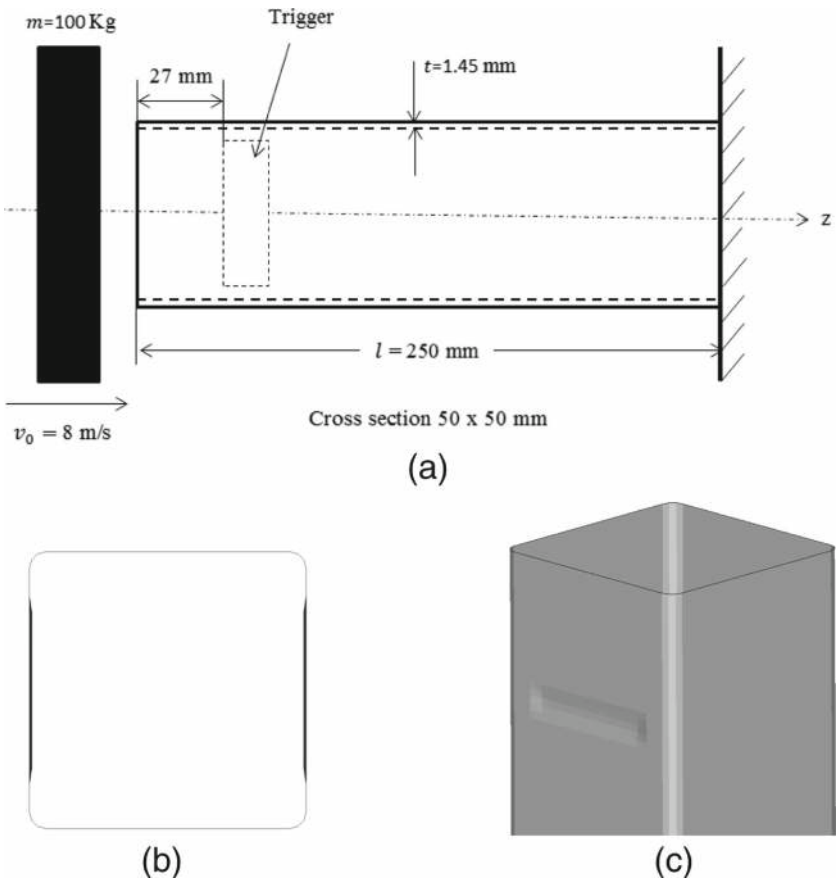

Fig. 15 **a** Schematic side view of square tube **b** top view and **c** iso-view showing trigger

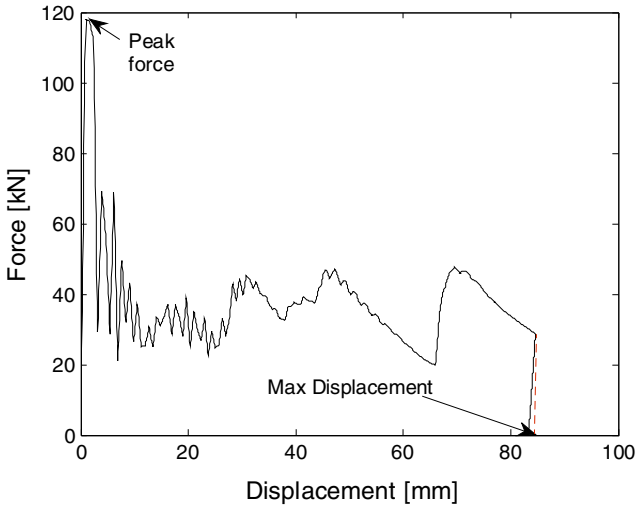

Fig. 17 Axial crushing force-displacement curve

5 Results

In this work, the accuracy of the previously presented seven approximative scatter modeling approaches has been evaluated. Firstly, the approximation methods are evaluated by comparing the approximated scatter of important material properties with the actual scatter obtained from the tensile tests. Secondly, the approximation methods are compared to the Direct method, considered to be the true result, using selected responses from an axially-crushed, square tube.

5.1 Material parameter variation

The estimates of variation in the material properties $R_{p0.2}$ and R_m by the approximation methods are presented in Table 2. The normalized absolute errors $E1(\mu)$) and $E1$ (σ) are used as the error indicators for the mean and standard deviation respectively, where

$$E1\ (\mu) = \frac{abs\left(\mu_y - \mu_{\hat{y}}\right)}{\mu_y} \tag{9}$$

$$E1\ (\sigma) = \frac{abs\left(\sigma_y - \sigma_{\hat{y}}\right)}{\sigma_y} \tag{10}$$

where μ_y and σ_y are the mean or the standard deviation of the material properties observed in the experiments, whereas $\mu_{\hat{y}}$ and $\sigma_{\hat{y}}$ are the estimates obtained by the approximating method. The estimated errors are presented in Table 3.

5.2 Response variation

The scatter in the structural responses obtained by using the methods studied is presented in Fig. 18. The mean and the standard deviation of each distribution are summarized in Table 4. The estimation errors for each of the approximation methods, *am*, as compared to the Direct method, *dm*, are evaluated using Eq. (11), which is assumed to illustrate a balanced total error. The errors computed are presented in Table 5.

$$E2 = \left\{ \frac{1}{4} \left[\left(\frac{D_{max}(dm) - D_{max}(am)}{D_{max}(dm)} \right)^2 + \left(\frac{\left(F_{peak}(dm) - F_{peak}(am) \right)}{F_{peak}(dm)} \right)^2 + \left(\frac{F_{avg}(dm) - F_{avg}(am)}{F_{avg}(dm)} \right)^2 + \left(\frac{AE(dm) - AE(am)}{AE(dm)} \right)^2 \right] \right\}^{\frac{1}{2}} \tag{11}$$

6 Discussion

This study evaluates the performance of some simple approximating material scatter modeling methods used to incorporate material scatter in stochastic simulations and stochastic design

Table 2 Material scatter data generated using approximation methods and as a reference the Direct method

	$R_{p0.2}$ [MPa] (true stress)		R_m [MPa] (true stress)	
	μ	σ	μ	σ
Direct method	378.94	13.77	743.75	15.98
Method 1a	461	20.20	735.1	32.22
Method 1b	461	13.08	735.1	20.87
Method 2a	379.8	16.65	741.5	32.50
Method 2b	379.8	10.78	741.5	21.05
Method 3	346.34	18.55	770.01	16.08
Method 4	327.54	12.48	NA	NA
Method 5	378.94	13.77	759.91	15.06

Table 3 Error measurement for the approximation models' material scatter estimation

Method	Estimation error [Normalized absolute error]			
	$R_{p0.2}$		R_m	
	μ	σ	μ	σ
Method 1a	0.217	0.47	0.012	1.02
Method 1b	0.217	0.05	0.012	0.31
Method 2a	0.002	0.21	0.003	1.03
Method 2b	0.002	0.22	0.003	0.32
Method 3	0.086	0.35	0.035	0.01
Method 4	0.136	0.09	NA	NA
Method 5	0	0	0.019	0.58

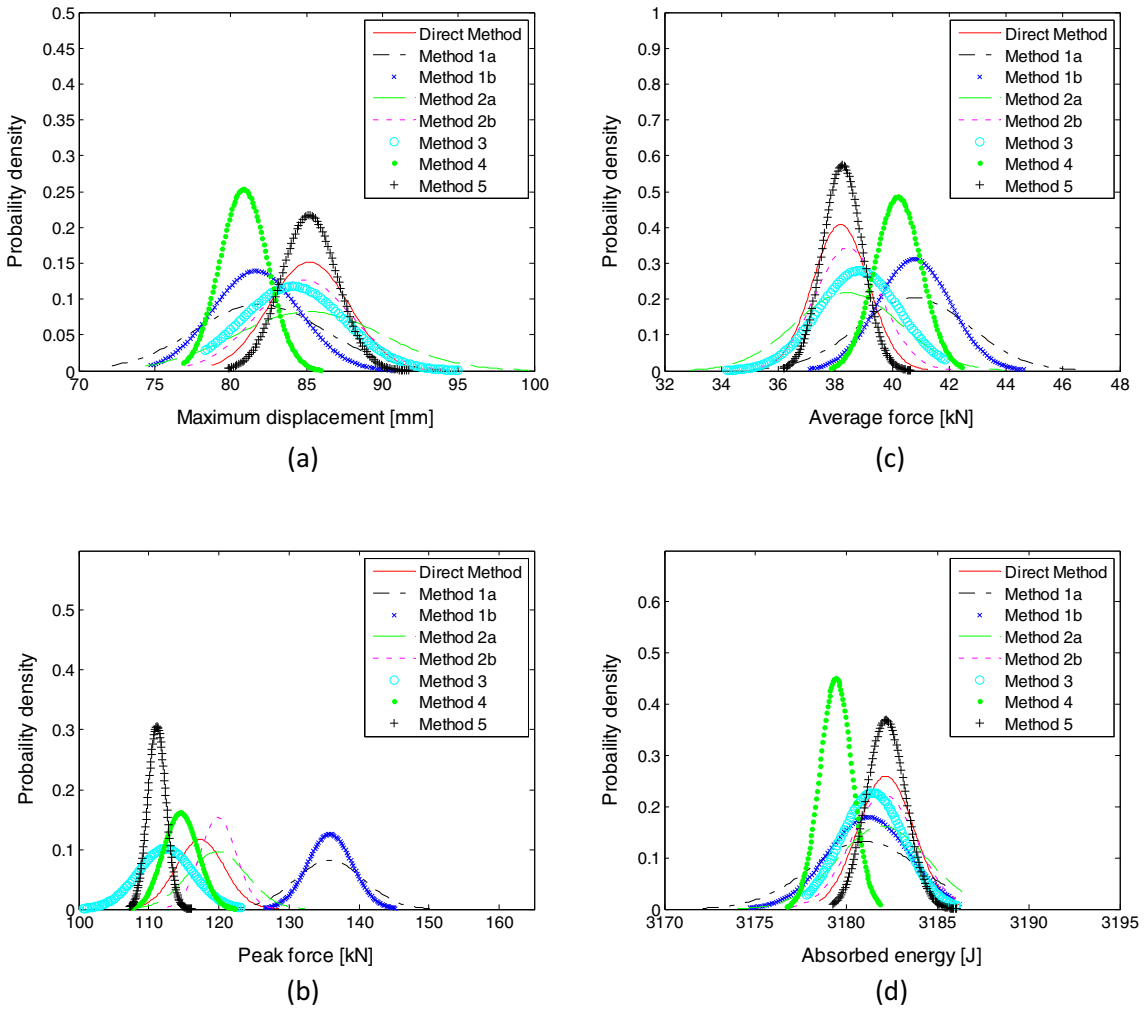

Fig. 18 Probability density function of the responses **a** Maximum displacement **b** Peak force **c** average force **d** Absorbed energy

optimizations at early product design stages. The evaluation is performed based on the variation of selected responses from an axially-crushed, thin-walled square tube. The results indicate that some of the approximate methods studied estimate the material scatter and the scatter in the responses reasonably well. As can be seen from Table 2 and Table 3, Method 1b has the lowest estimation error for the standard deviation of $R_{p0.2}$. However the estimate of the mean $R_{p0.2}$ using this method is poor. The estimate of the standard deviation of R_m provided by Method 3 is better than the other methods. The overall error

Table 4 Stochastic analysis results

	Max displacement [mm]		Peak Force [kN]		Average Force [kN]		Absorbed Energy [J]	
Method	μ	σ	μ	σ	μ	σ	μ	σ
Nominal	84.57		117.92		38.39		3781.89	
Direct method	85.19	2.62	117.3	3.42	38.18	0.98	3182.2	1.53
Method 1a	81.93	4.31	135.7	4.87	40.76	1.95	3181.0	3.02
Method 1b	81.66	2.86	135.8	3.17	40.77	1.27	3181.2	2.22
Method 2a	85.17	4.83	119.7	4.13	38.42	1.83	3182.0	2.46
Method 2b	84.82	3.14	119.9	2.60	38.44	1.61	3182.3	1.78
Method 3	84.08	3.39	112.4	3.94	38.84	1.43	3181.4	1.76
Method 4	80.83	1.57	114.5	2.46	40.19	0.82	3179.4	0.89
Method 5	85.18	1.84	111.15	1.30	38.23	0.70	3182.2	1.08

Table 5 Error measurement for the approximation models' response variation

	Estimation error (E)	
	μ	σ
Method 1a	0.088	0.798
Method 1b	0.088	0.278
Method 2a	0.011	0.688
Method 2b	0.012	0.370
Method 3	0.024	0.296
Method 4	0.039	0.332
Method 5	0.026	0.282

measurement for material scatter estimation indicates that Method 2b and Method 3 perform better than the other methods. Since it is not possible to locate R_m for each stress–strain curve in Method 4, the R_m scatter estimates for this method are not presented in the table. In Method 5, the R_m scatter is generated using $R_{p0.2}$ distribution from the test data. Therefore in Table 3 the estimation error is zero for the $R_{p0.2}$ estimation.

Table 5 shows that Method 2b, Method 3, Method 4 and Method 5 perform reasonably well in estimating the response variation collectively as compared to the other methods. Table 4 shows that Method 5 is poor in estimating the variation in peak force and Method 4 gave poor estimation of the max displacement variation.

The overall results indicate that Method 2b, Method 3, Method 4 and Method 5 provide reasonable estimates of the mean and variation of the responses, see Table 4 and Fig. 18. Method 2b and Method 3 also provide better estimates of the scatter in material properties compared to the other methods, cf. Table 2. Although the performance of the methods in estimating response variations is not directly related to their performance in estimating the scatter in the material properties R_m and $R_{p0.2}$, the methods that have performed better in estimating response variations have also performed well in estimating the scatter in the material properties R_m and $R_{p0.2}$. The type and amount of scatter data required by these methods varies. Method 4 and Method 5 are expensive compared to the other two methods since they require a significant amount of experimental data, whereas, Method 2b and Method 3 require a minimal amount of experimental data. Method 2b requires the nominal stress–strain curve based on a tensile test in addition to standard material data. Method 3 requires information regarding scatter in the strain hardening exponent, n, as well as standard material data.

In general, both the location and the spread in the data are important in robustness analysis, consequently both the mean and the standard deviation estimates are equally important for an accurate scatter representation. The reason for the poor estimates of the mean of the responses by Method 1a, Method 1b and Method 4 is likely the fitting error. As can be seen from Fig. 6, the fitted analytical curve in Method 1 differs from the nominal stress–strain curve of the Direct method. Similarly, Fig. 13 shows that there is a difference between the average curve obtained by using Method 4 and the nominal stress–strain curve from the Direct method, especially in the region beyond the necking point. The primary reason for the poor fitting in Method 1 is the fact that the minimum value of n is used since that is the only data provided in the material specification instead of the nominal n. Method 1b or Method 4 would have performed better if the analytical curve used in these methods had captured the stress–strain relation of the experimental stress–strain curve of the material used.

The results from Method 1 and Method 2 indicate that scaling stress–strain curve based on R_m scatter yields better estimates of scatter in the responses than the scaling based on the $R_{p0.2}$ scatter. As can be seen in Table 4 and Fig. 18, Method 1a and Method 2a overestimate the variation in the responses. The main reason, in both cases, is that the scaling factors are based on $R_{p0.2}$ scatter and the magnitude of $R_{p0.2}$ is small compared to R_m. Consequently, the scaled curves grow into a much wider spectrum than the spectrum of the actual hardening curves from the experiments, especially at higher strains, see Fig. 7 and Fig. 9. The scatter estimates using Method 1b and Method 2b are much better than those of Method 1a and Method 2a. This is due to the fact that the width of the scaled curves spectrum obtained by this method nearly matches the test curve spectrum, see Figs. 8 and 10.

The Direct method is based on 102 tensile test curves and it is found that the number of samples is adequate to capture the variation in the material properties with a sufficient accuracy according to the confidence intervals of the estimated mean and standard deviation of mechanical properties, see Table 1. It should be noted that no additional physical tests were performed in order to obtain the strain hardening values beyond the necking point. Instead, the strain hardening functions beyond necking are fitted to the tensile test using inverse analysis.

The tensile test curve, which approximately represents the average of the test curves has been used as the nominal stress–strain curve in Method 2. The nominal stress–strain curve provided by material suppliers usually represents the average tensile test curve. If the nominal stress–strain curve provided by the supplier does not represents the average curve, the scaling factors range needs to be adjusted. The scaling factor range can be computed by using the stress interval of the standard data and the stress level ($R_{p0,2}$ *or* R_m) of the given nominal curve.

7 Conclusion

In this work, the accuracy of commonly-used, simplified methods to model scatter in material properties is evaluated by comparing material scatter generated by these methods to the material scatter obtained by complete tensile tests. Furthermore, the methods are compared based on selected responses from an axially-crushed, square tube made from DP600 steel. The impact load case is considered in this study, since this type of load condition is critical in vehicle body structure development.

The overall results show that Method 2b, Method 3, Method 4 and Method 5 provide higher levels of accuracy compared to the other scatter modeling approaches. Method 4 and Method 5 require a significant amount of experimental data, whereas Method 3 and Method 2b require a minimal amount of experimental data apart from standard material data. Method 2b is the most economical and pragmatic in the early stages of a design process and the accuracy level provided by this method is sufficient for the early design studies. As long as the strain hardening behavior of the stress–strain curves of the material does not vary much as compared to the nominal hardening curve, this method will estimate the variation in responses reasonably well. If scaling of the stress–strain relation is used to describe the material scatter, then the use of scaling factors based on the R_m scatter is recommended. The conclusion provided is based on responses of an impact load case involving DP 600 material.

Acknowledgements We would like to thank Dr. Mikael Fermér and Dr. Alexander Govik of Volvo Car Corporation for their support throughout this project. This work has been carried out with financial support from the 'Robust and multidisciplinary optimization of automotive structures' Project funded by Vinnova FFI and Volvo Car Corporation.

References

Abedrabbo N, Mayer R, Thompson A, Salisbury C, Worswick M, van Riemsdijk I (2009) Crash response of advanced high-strength steel tubes: experiment and model. Int J Impact Eng 36(8):1044–1057

Anderson TW, Darling DA (1952) Asymptotic theory of certain" goodness of fit" criteria based on stochastic processes. The annals of mathematical statistics:193–212

Aspenberg D, Nilsson L, Jergeus J (2013) Robust optimization of front members in a full frontal car impact. Eng Optim 45(3):245–264

Chen P, Koç M (2007) Simulation of springback variation in forming of advanced high strength steels. Int J Mater Prod Technol 190(1–3): 189–198

Cohen J (1988) Statistical Power Analysis for the Behavioral Sciences. L. Erlbaum Associates

Del Prete A, Primo T, Strano M (2010) The use of FEA packages in the simulation of a drawing operation with springback, in the presence of random uncertainty. Finite Elem Anal Des 46(7):527–534

Embrechts P, Lindskog F, McNeil A (2001) Modelling dependence with copulas. Rapport technique, Département de mathématiques, Institut Fédéral de Technologie de Zurich, Zurich

Even D, Reichert B (2010) A pragmatic strategy to take into account metal materials scatter in FEA. In: Forum L-D (ed) Proceedings of 9th German LS-DYNA Forum. Bamberg, Germany

Haldar A, Mahadevan S (2000) Probability, reliability and statistical methods in engineering. John Wiley & Sons, Design

Hallquist JO (2006) LS-DYNA Theory Manual. Livermore Software Technology Corporation

Jansson T, Nilsson L, Moshfegh R (2008) Reliability analysis of a sheet metal forming process using Monte Carlo analysis and metamodels. J Mater Process Technol 202(1–3):255–268

Larsson R, Björklund O, Nilsson L, Simonsson K (2011) A study of high strength steels undergoing non-linear strain paths-experiments and modelling. J Mater Process Technol 211(1):122–132

Ledoux Y, Sergent A, Arrieux R (2007) Impact of the material variability on the stamping process: numerical and analytical analysis. In: Numiform 07, Porto, Portugal, June 17–21 2007. AIP Conference Proceedings Volume 908. pp 1213–1218

Lee M-G, Kim D, Kim C, Wenner ML, Chung K (2005) Spring-back evaluation of automotive sheets based on isotropic–kinematic hardening laws and non-quadratic anisotropic yield functions, part III: applications. Int J Plast 21(5):915–953

Li X, Olpak T, Högberg A (2009) Robustness and optimization of rear bumper beam. Master thesis, KTH Royal Institute of Technology, Stockholm, Sweden

Lönn D, Öman M, Nilsson L, Simonsson K (2009) Finite element based robustness study of a truck cab subjected to impact loading. Int J Crashworthiness 14(2):111–124

Marretta L, Di Lorenzo R (2010) Influence of material properties variability on springback and thinning in sheet stamping processes: a stochastic analysis. Int J Adv Manuf Technol 51(1–4):117–134

Müllerschön H, Lorenz D, Roll K (2007) Reliability based design optimization with LS-OPT for a metal forming application. In: Proceedings of 6th German LS-DYNA Forum Frankenthal, Germany, October 11–12 2007.

Quetting F, Hora P, Roll K (2012) Modelling of strain hardening behaviour of sheet metals for stochastic simulations. Key Eng Mater 504(1):41–46

Sigvant M, Carleer B (2006) Influence on simulation results from material and process scatter. In: Proceedings of the IDDRG 2006 Conference, Porto, Portugal, June 19–21 2006

VDA (2011) VDA 239–100 material specifications. German association of the automotive industry. Germany, Berlin

Wiebenga JH, Atzema EH, An YG, Vegter H, van den Boogaard AH (2014) Effect of material scatter on the plastic behavior and stretchability in sheet metal forming. Int J Mater Prod Technol 214:238–252